Generalized Multilayer Anisotropic Dielectric Resonators

Chi Wang, *Senior Member, IEEE,* and Kawthar A. Zaki, *Fellow, IEEE*

***Abstract*—Modeling of the generalized multilayer cylindrical anisotropic dielectric loaded resonator by a rigorous mode-matching method is presented in this paper. Eigenmodes of the multilayer two parallel-plate waveguides are obtained. By cascading the radial discontinuities of the structure, resonant frequency, field distribution, unloaded Q, and the frequency sensitivity of the resonator are obtained. The method can be used to analyze and design resonators and filters of multilayer structure. The computed results are compared with the results in [13] and with experimental data, and is shown to be in good agreement.**

I. Introduction

With THE breakthrough of the ceramic technology, a number of new high dielectric-constant materials with a high-quality factor low- temperature coefficient were developed. Tremendous progress on stabilization and miniaturization of resonators and filters has been achieved over the past three decades. Dielectric loaded resonators and filters with high unloaded Q have been widely used in communication systems and other microwave applications [1]–[5].

Cooled ultra-high Q high- stability sapphire dielectric resonators operating at a whispering-gallery mode (WGM) (a hybrid mode with a large number of azimuthal variations) found important applications in the construction of ultra-stable low-noise microwave oscillators [5]–[12], [14]. Since single crystalline sapphire is a dielectric with uniaxial anisotropy, the influence of the anisotropic dielectric constants on the resonant modes of the resonator needs to be considered [12]. The support of the dielectric loaded resonator is needed to improve the reliability of the resonator. Thus, the effects of the support structure on the resonant frequencies and unloaded Q of the resonator should be taken into account in the resonator design [14].

Recently, there has been increasing interest in the design of tunable dielectric loaded resonators and filters. Some applications require the use of a dielectric loaded resonator of very complicated structure. An accurate and efficient computer simulation tool to compute the resonant-frequency, unloaded Q, and field distribution is essential in the resonator design. It is neither efficient nor convenient to develop a dedicated computer program for each configuration of dielectric loaded resonator. A generalized structure that can fit as many configurations as possible would be very desirable to satisfy the need of future work. Thus, a modeling method for analysis of the generalized isotropic and uniaxial anisotropic multilayer dielectric loaded resonator structure needs to be developed for design of the sapphire and other multilayer dielectric loaded resonators and filters.

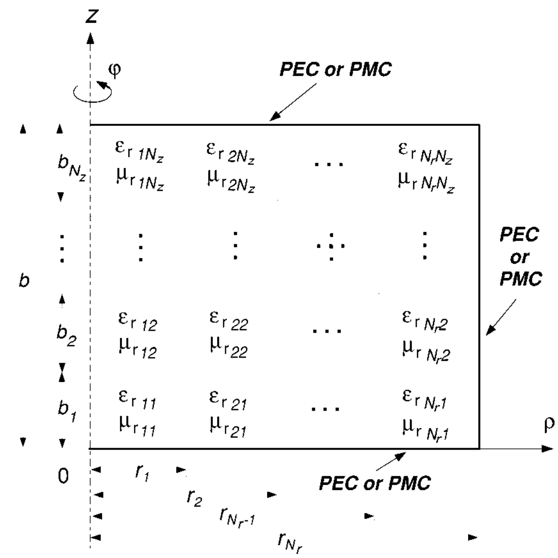

Fig. 1. Configuration of the generalized multilayer cylindrical uniaxial-anisotropic dielectric loaded resonator.

In this paper, the modeling of the generalized multilayer cylindrical uniaxial anisotropic dielectric loaded resonator by a rigorous radial mode-matching method is presented. Resonant-frequency field distribution and the unloaded Q for all resonant modes of the resonator of arbitrary dimension can be accurately determined. The resonant-frequency sensitivity to the enclosure dimension changes is computed by using the perturbation theory. The configuration of the resonator is general, which allows many types of the isotropic and uniaxial anisotropic resonators to be analyzed and designed. The correctness of the method is verified by comparing its results with the computed results in [13] and the measured data, and is shown to be in good agreement.

II. Configuration and Theory

The configuration of a generalized multilayer cylindrical uniaxial-anisotropic dielectric loaded resonator under consideration is shown in Fig. 1 in a cylindrical coordinate system (ρ, ϕ, z). There are N_z layers in the z-direction and N_r layers in the r-direction. Therefore, the structure can be partitioned into $N_z \times N_r$ regions to be analyzed by the mode-matching method.

Manuscript received October 8, 1998.

C. Wang was with the Department of Electrical Engineering, University of Maryland at College Park, College Park, MD 20742 USA. He is now with Celwave Inc., Marlboro, NJ 07746 USA.

K. A. Zaki is with the Department of Electrical Engineering, University of Maryland at College Park, College Park, MD 20742 USA.

Publisher Item Identifier S 0018-9480(00)00212-X.

Each region can be filled with a uniaxial-anisotropic dielectric material with the relative permittivity tensor $(\bar{\epsilon}_r)_{ij}$, loss tangent $(\tan\delta)_{ij}$, and relative isotropic permeability $(\mu_r)_{ij}$. The enclosure's top wall, bottom wall, and sidewalls can be either perfect electric conductor (PEC) or perfect magnetic conductor (PMC).

The permittivity tensor $\bar{\epsilon}_r$ is given by

$$\bar{\epsilon}_r = \begin{bmatrix} \epsilon_t & 0 & 0 \\ 0 & \epsilon_t & 0 \\ 0 & 0 & \epsilon_z \end{bmatrix}. \tag{1}$$

For the isotropic case, the dielectric constants ϵ_t and ϵ_z are equal. Since the number of layers N_z, N_r of the resonator are arbitrary and the dielectric constant in each region can also be chosen arbitrarily, the configuration is very general and allows almost unlimited types of structures to be analyzed.

Starting from Maxwell's equations, the wave equations in the charge-free uniaxial anisotropic medium can be obtained as [13]

$$\nabla^2 \vec{E} - \left(1 - \frac{\epsilon_z}{\epsilon_t}\right) \nabla \left(\frac{\partial E_z}{\partial z}\right) + k_o^2 \mu_r \epsilon_z \vec{E} = 0 \tag{2}$$

$$\nabla^2 \vec{H} - j\omega\epsilon_o\epsilon_t \left(1 - \frac{\epsilon_z}{\epsilon_t}\right) \nabla \times (\hat{z} E_z) + k_o^2 \mu_r \epsilon_t \vec{H} = 0. \tag{3}$$

Since the components of $\vec{E}$ and $\vec{H}$ are not all independent, it is not necessary to solve all six scalar wave equations for the six field components at the same time. To simplify the analysis, it is usual to decompose the normal mode fields into two orthogonal sets of solutions, i.e., TE_z modes ($E_z = 0$) and TM_z modes ($H_z = 0$) by solving the z component wave equations only. The total electromagnetic fields are, therefore, the summation of the eigenmode fields of both sets. The transverse electromagnetic fields in each region can then be expressed as

$$\begin{aligned} \vec{E}_t^p(\rho, \phi, z) &= \sum_j^{N_p^e} \left\{ C_j^{pe} \mathcal{B}_{CEj}^{pe}(\rho) + D_j^{pe} \mathcal{B}_{DEj}^{pe}(\rho) \right\} \times \vec{e}_{tj}^{pe}(\rho, \phi, z) \\ &\quad + \sum_j^{N_p^h} \left\{ C_j^{ph} \mathcal{B}_{CEj}^{ph}(\rho) + D_j^{ph} \mathcal{B}_{DEj}^{ph}(\rho) \right\} \times \vec{e}_{tj}^{ph}(\rho, \phi, z) \end{aligned} \tag{4}$$

$$\begin{aligned} \vec{H}_t^p(\rho, \phi, z) &= \sum_j^{N_p^e} \left\{ C_j^{pe} \mathcal{B}_{CHj}^{pe}(\rho) + D_j^{pe} \mathcal{B}_{DHj}^{pe}(\rho) \right\} \times \vec{h}_{tj}^{pe}(\rho, \phi, z) \\ &\quad + \sum_j^{N_p^h} \left\{ C_j^{ph} \mathcal{B}_{CHj}^{ph}(\rho) + D_j^{ph} \mathcal{B}_{DHj}^{ph}(\rho) \right\} \times \vec{h}_{tj}^{ph}(\rho, \phi, z) \end{aligned} \tag{5}$$

where N_p^e and N_p^h are the number of TE and TM modes used in region p, $p = 1, \ 2, \cdots, N_r$, respectively, C_j^{pe}, D_j^{pq} are the field coefficients in each region, $\mathcal{B}_{Ej}^{pe}$, $\mathcal{B}_{Hj}^{ph}$, $\mathcal{B}_{Hj}^{pe}$, and $\mathcal{B}_{Ej}^{ph}$ are the first- and second-kind Bessel functions, and J_n, Y_n, or associated Bessel functions I_n, K_n. $\vec{e}_{tj}^{pq}$, $\vec{h}_{tj}^{pq}$ are the transverse eigenfields of the TE mode ($q = h$) or TM mode ($q = e$) of the multilayer uniaxial anisotropic dielectric loaded two parallel-plate radial waveguide bounded in the z-direction, and are given as

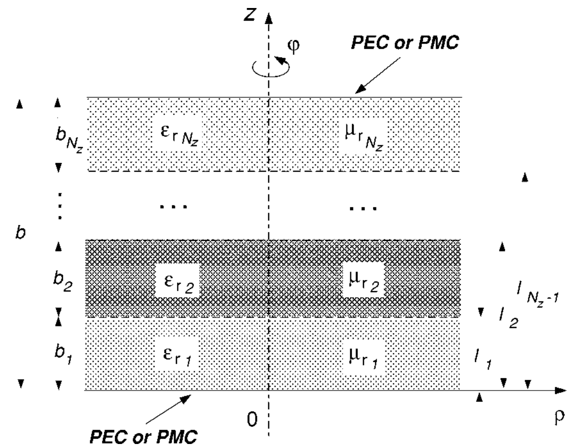

Fig. 2. Configuration of the multilayer uniaxial anisotropic two parallel-plate radial waveguide.

$$\begin{aligned} \vec{e}_{tj}^{pe}(\rho, \phi, z) &= \hat{z} \begin{Bmatrix} \sin(n\phi) \\ \cos(n\phi) \end{Bmatrix} e_{zj}^{pe}(\gamma_j^{pe}, z) \\ &\quad - \hat{\phi} \frac{1}{\xi_j^{pe\,2}} \frac{n}{\rho} \begin{Bmatrix} \cos(n\phi) \\ -\sin(n\phi) \end{Bmatrix} \\ &\quad \times \frac{\epsilon_z^p}{\epsilon_t^p} \frac{\partial}{\partial z} e_{zj}^{pe}(\gamma_j^{pe}, z) \end{aligned} \tag{6}$$

$$\vec{e}_{tj}^{ph}(\rho, \phi, z) = \hat{\phi} \frac{\mu_r^p}{\xi_j^{ph\,2}} \begin{Bmatrix} \cos(n\phi) \\ -\sin(n\phi) \end{Bmatrix} h_{zj}^{ph}(\gamma_j^{ph}, z) \tag{7}$$

$$j\omega\mu_o \vec{h}_{tj}^{pe}(\rho, \phi, z) = \hat{\phi} \frac{k_o^2 \epsilon_z^p}{\xi_j^{pe\,2}} \begin{Bmatrix} \sin(n\phi) \\ \cos(n\phi) \end{Bmatrix} e_{zj}^{pe}(\gamma_j^{pe}, z) \tag{8}$$

$$\begin{aligned} j\omega\mu_o \vec{h}_{tj}^{ph}(\rho, \phi, z) &= \hat{z} \begin{Bmatrix} \cos(n\phi) \\ -\sin(n\phi) \end{Bmatrix} h_{zj}^{ph}(\gamma_j^{ph}, z) \\ &\quad - \hat{\phi} \frac{1}{\xi_j^{ph\,2}} \frac{n}{\rho} \begin{Bmatrix} \sin(n\phi) \\ \cos(n\phi) \end{Bmatrix} \\ &\quad \times \frac{\partial}{\partial z} h_{zj}^{ph}(\gamma_j^{ph}, z) \end{aligned} \tag{9}$$

$$\xi^{e\,2} = \frac{\epsilon_z}{\epsilon_t} \gamma^{e\,2} + k_o^2 \mu_r \epsilon_z \tag{10}$$

$$\xi^{h\,2} = \gamma^{h\,2} + k_o^2 \mu_r \epsilon_t \tag{11}$$

where ξ_j^{ph}, ξ_j^{pe} are the wavenumbers of the TE and TM modes in the corresponding region, $h_z^h(\gamma_z^h, z)$ and $e_z^e(\gamma_z^e, z)$ are the TE_z and TM_z mode's eigenfunctions of the multilayer two parallel-plate radial waveguide in each of the layers shown in Fig. 2, and relating the ξ^q and γ^q by the differential equations as

$$\frac{\partial^2}{\partial z^2} e_z^e(\gamma_z^e, z) - \gamma^{e\,2} e_z^e(\gamma_z^e, z) = 0 \tag{12}$$

and

$$\frac{\partial^2}{\partial z^2} h_z^h(\gamma_z^h, z) - \gamma^{h\,2} h_z^h(\gamma_z^h, z) = 0. \tag{13}$$

The general solutions of (12) and (13) in each layer are given as

$$\left\{ \begin{array}{l} e_i^{e_z}(\gamma_i^{e_z}, z) \\ h_i^{h_z}(\gamma_i^{h_z}, z) \end{array} \right\} = \mathcal{C}_{s_i} sh(\gamma_{z_i}^{e,h} z - a_i) + \mathcal{C}_{c_i} ch(\gamma_{z_i}^{e,h} z - a_i) \tag{14}$$

where a_i can be set as $a_1 = 0$, $a_i = l_i$, ($i = 2$ to $N_z - 1$), and $a_{N_z} = b$; $\mathcal{C}_{s_i}, \mathcal{C}_{c_i}$ are coefficients of the eigenfunction in each layer, and one of the coefficients of the top and bottom layers is zero due to the boundary condition of the plates.

The boundary conditions at the interfaces between the layers require that the tangential electromagnetic fields to be continuous, and are relating to the normal fields as follows.

For TE_z mode:

$$\mu_{r_i} h_{z_i}^h(\gamma_{z_i}^h, z)|_{z=l_i} = \mu_{r_{i+1}} h_{z_{i+1}}^h(\gamma_{z_{i+1}}^h, z)|_{z=l_i} \tag{15}$$

$$\left.\frac{\partial h_{z\,i}^h(\gamma_{z\,i}^h, z)}{\partial z}\right|_{z=l_i} = \left.\frac{\partial h_{z\,i+1}^h(\gamma_{z\,i+1}^h, z)}{\partial z}\right|_{z=l_i}. \tag{16}$$

For TM_z mode:

$$\epsilon_{r_{z_i}} e_{z_i}^e(\gamma_{z_i}^e, z)\big|_{z=l_i} = \epsilon_{r_{z_{i+1}}} e_{z_{i+1}}^e(\gamma_{z_{i+1}}^e, z)\big|_{z=l_i} \tag{17}$$

$$\left.\frac{\epsilon_{r_{z_i}}}{\epsilon_{r_{t_i}}} \frac{\partial e_{z_i}^e(\gamma_{z_i}^e, z)}{\partial z}\right|_{z=l_i} = \left.\frac{\epsilon_{r_{z_{i+1}}}}{\epsilon_{r_{t_{i+1}}}} \frac{\partial e_{z_{i+1}}^e(\gamma_{z_{i+1}}^e, z)}{\partial z}\right|_{z=l_i}$$

$$i = 1, 2, \cdots, N_{z-1}. \tag{18}$$

The field coefficients of the layers can be related to each other by substituting the field expressions of each layer into the boundary-condition equations. Eliminating the coefficient $\mathcal{C}_{s_{N_z}}^h$ or $\mathcal{C}_{c_{N_z}}^h$ of the last layer's field continuity equations, a characteristic equation for the radial propagation constant ξ^h of the eigenmodes containing the field coefficients $\mathcal{C}_{s\,N_z-1}^p$, and $\mathcal{C}_{c\,N_z-1}^p$ of the $N_z - 1$ layer can finally be obtained.

For a given frequency, the value ξ^p satisfying the characteristic equation gives the propagation constant of the two parallel-plate waveguide's eigenmode, where $\gamma_{z_i}^p$ can be obtained from ξ^p, $p = h$, or e. The field coefficients $\mathcal{C}_{s_{N_{z-1}}}^p$ and $\mathcal{C}_{c_{N_{z-1}}}^p$ can be obtained by repeatedly computing the $\mathcal{C}_s^p$ and $\mathcal{C}_c^p$ of the previous layers from the boundary-condition equations. By assigning a nonzero value to $\mathcal{C}_{s_1}^p$ or $\mathcal{C}_{c_1}^p$, all the field coefficients of the two parallel-plate waveguide's eigenfunction can be determined.

Having obtained the eigenfunctions in the z-direction and all the field components of the eigenmodes of the multilayer uniaxial-anisotropic dielectric loaded two parallel-plate radial waveguides, a rigorous radial mode-matching method is then applied to solve the discontinuity between the multilayer structure in the radial direction. There are N_r radial regions in the resonator, and each radial region has N_z layer dielectrics in the z-direction. Fig. 3 shows the radial discontinuity between the i and $i + 1$ layer of the resonator. Solving the generalized i and $i + 1$ layer radial discontinuity, the total of $N_r - 1$ discontinuities in the resonator can then be obtained. As a result, all the field coefficients of the eigenmodes can be determined.

The boundary conditions at the interface between two multilayer radial waveguide regions at $\rho = r_i$ gives

$$\vec{E}_t^i(\rho = r_i, \phi, z) = \vec{E}_t^{i+1}(\rho = r_i, \phi, z) \tag{19}$$

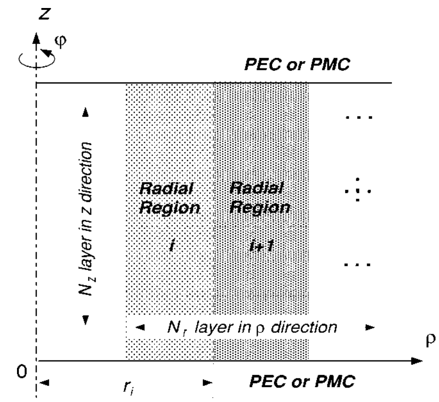

Fig. 3. Configuration of the radial discontinuity in the dielectric loaded resonator.

and

$$\vec{H}_t^i(\rho = r_i, \phi, z) = \vec{H}_t^{i+1}(\rho = r_i, \phi, z) \tag{20}$$

where i is the inner region and $i+1$ is the outer region. The inner product of two fields at the interface of the regions is defined as [4]

$$\langle \vec{e}^{p_1}, \vec{h}^{p_2} \rangle = \int_S \vec{e}^{p_1} \times \vec{h}^{p_2} \cdot \hat{\rho}\, dS = \iint_{S^S} (e_\phi^{p_1} h_z^{p_2} - e_z^{p_1} h_\phi^{p_2})\, \rho\, d\phi\, dz. \tag{21}$$

Taking the inner product of the electric-field boundary condition (19) with the magnetic transverse eigenfield $\vec{h}^{i+1}$ in the outer region, and the inner product to the magnetic field boundary condition (20) with the electric transverse eigenfield $\vec{e}^i$ in the inner region, the equations relating the field coefficients of the two regions due to the discontinuity can be obtained as follows:

$$\left[\langle \vec{e}^i, \vec{h}^{i+1} \rangle\right] \left\{ [\mathcal{B}_{CE}^i][C^i] + [\mathcal{B}_{DE}^i][D^i] \right\} = \left[\langle \vec{e}^{i+1}, \vec{h}^{i+1} \rangle\right] \left\{ [\mathcal{B}_{CE}^{i+1}][C^{i+1}] + [\mathcal{B}_{DE}^{i+1}][D^{i+1}] \right\} \tag{22}$$

and

$$\left[\langle \vec{e}^i, \vec{h}^i \rangle\right] \left\{ [\mathcal{B}_{CH}^i][C^i] + [\mathcal{B}_{DH}^i][D^i] \right\} = \left[\langle \vec{e}^i, \vec{h}^{i+1} \rangle\right]^T \left\{ [\mathcal{B}_{CH}^{i+1}][C^{i+1}] + [\mathcal{B}_{DH}^{i+1}][D^{i+1}] \right\}. \tag{23}$$

Consider the discontinuity between the radial region i and region $i+1$. Assume that the field coefficient matrix $[T_{CD}^i]$ of the inner region i is known from solving the discontinuity of the previous region as

$$[D^i] = [T_{CD}^i][C^i]. \tag{24}$$

Substitute (24) into (22) and (23), the field coefficient relation matrix of the outer region $i+1$ can then be obtained as follows:

$$[D^{i+1}] = [T_{CD}^{i+1}][C^{i+1}] \tag{25}$$

where

$$[T_{CD}^{i+1}] = \left\{ [\lambda^{i+1}][\mathcal{B}_{DE}^{i+1}] - [A][\mathcal{B}_{DH}^{i+1}] \right\}^{-1} \times \left\{ [A][\mathcal{B}_{CH}^{i+1}] - [\lambda^{i+1}][\mathcal{B}_{CE}^{i+1}] \right\} \tag{26}$$

$$[A] = [M^{i+1,i}]\left\{[\mathcal{B}^i_{CE}] + [\mathcal{B}^i_{DE}][T^i_{CD}]\right\} \times \left\{[\lambda^i][\mathcal{B}^i_{CH}] + [\lambda^i][\mathcal{B}^i_{DH}][T^i_{CD}]\right\}^{-1} \times [M^{i+1,i}]^T \tag{27}$$

$$[M^{p_2,p_1}] = \left[\langle \vec{e}^{p_1}, \vec{h}^{p_2}\rangle\right] \tag{28}$$

$$[\lambda^p] = \left[\langle \vec{e}^{p}, \vec{h}^{p}\rangle\right]. \tag{29}$$

Since all the elements of the field coefficient matrix $[T^1_{CD}]$ of the inner most region that contains the point $\rho = 0$ are zero, the coefficient matrix $[T^2_{CD}]$ can then be obtained. Repeated cascading of the coefficient matrices from inside to outside of the dielectric loaded resonator results in an equation relating the field coefficients of the outer most region

$$[M^{N_r}_C][C^{N_r}] + [M^{N_r}_D][D^{N_r}] = 0. \tag{30}$$

Applying the boundary conditions at the side enclosure wall $\rho = r_{N_r}$, the characteristic equation for the resonant frequency of the resonator can finally be obtained. The determinant of the equation must be zero for nontrivial solutions

$$\det[X]_{N_{N_r} \times N_{N_r}} = 0 \tag{31}$$

$$[X] = [M^{N_r}_C] + [M^{N_r}_D][T^{N_r}_{CD}]. \tag{32}$$

Searching for the frequencies that are zeros of the determinant of the characteristic equation give the resonant frequencies of the modes of the uniaxial anisotropic dielectric loaded resonator. Solving the characteristic equation and the field continuity equations at the interfaces of the dielectric layers, the field coefficients in each layer of the whole resonator can be obtained.

The computation of the unloaded Q involves the calculation of the stored energy $W_{E,H}$ of the resonant mode in the structure, dielectric loss P_d, and conductor losses P_c at the enclosure. Since all the eigenmode functions and their field coefficients are known, the above computation can be achieved analytically, which yields high computational efficiency and accuracy, especially for WGM resonators. The total unloaded Q of the resonator is computed from

$$\frac{1}{Q_u} = \frac{1}{Q_d} + \frac{1}{Q_c} = \frac{1}{\omega_o \dfrac{W_{E,H}}{P_d}} + \frac{1}{\omega_o \dfrac{W_{E,H}}{P_c}}. \tag{33}$$

The separation of Q_d and Q_c helps to understand the loss mechanism of the structure and to optimize the dimensions of the resonator.

For the WGM resonator, the resonant frequency is highly insensitive to the enclosure dimension of the resonator. To compute frequency dependence on resonator enclosure dimensions, it is possible to compare the changes of the resonant frequencies at two different enclosure dimensions. However, this method is quite unreliable and sometimes incorrect because it introduces large numerical errors. The accuracy of the results can be significantly improved by using the perturbation theory, which relates the changes in the resonant frequency Δf to the perturbation of the stored energy in the enclosure volume as

TABLE I
COMPARISON OF COMPUTED RESONANT FREQUENCIES (IN GIGAHERTZ) WITH THE NUMERICAL RESULTS AND MEASUREMENT OF A SOLID SAPPHIRE RESONATOR WITH $r_1 = 5.001$ mm, $r_2 = 7.775$ mm, $b_2 = 5.002$ mm, $b = 13.00$ mm, $\epsilon_{t11} = \epsilon_{t13} = 1.031$, $\epsilon_{t12} = 9.399$, and $\epsilon_{z12} = 11.553$

Mode	Present	Computed [13]	Measured
HE_{11}	9.8402	9.841	9.795
TM_{01}	10.6634	10.664	10.577
TE_{01}	10.7035	10.704	10.706
HE_{12}	12.1534	12.153	12.138

$$\frac{\Delta f}{f_0} = \frac{\int_{\Delta\tau} (\epsilon E^2 - \mu H^2)\, d\tau}{4W} \tag{34}$$

where $\Delta\tau$ is the perturbed volume of the resonator and W is the stored energy of the resonant mode.

For the resonator configuration considered, the frequency sensitivity problem can be divided into computation of the top and bottom plane sensitivity and sidewall sensitivity. Since there are neither tangential electric fields nor normal magnetic fields on the surface of the conductor, the frequency sensitivity of the resonator on height change Δb and radius change ΔR of the enclosure can be expressed as

$$\frac{\Delta f}{\Delta b} = \frac{\int_S [\epsilon_o E_z^2 - \mu_o (H_\rho^2 + H_\phi^2)]\, dS}{4W} f_0 \tag{35}$$

$$\frac{\Delta f}{\Delta R} = \frac{\int_S [\epsilon_o E_\rho^2 - \mu_o (H_z^2 + H_\phi^2)]\, dS}{4W} f_0 \tag{36}$$

where S is the perturbed area of top, bottom plane, or sidewall of the sapphire resonator. All the integrations needed for the frequency sensitivity computation can be evaluated analytically.

III. NUMERICAL RESULTS

A computer program has been developed to compute the resonant frequency, field distribution, unloaded Q, and frequency sensitivity of the cylindrical multilayer uniaxial anisotropic dielectric loaded resonators.

The convergence test of the computed results was first made to determine how many modes are required to achieve a certain accuracy. Extensive tests show that the results converge rapidly with the increase of the number of eigenmodes used, and the accuracy of the results within 0.05% can be achieved when the number of TE_z and TM_z modes is larger than eight for most of the dielectric resonator dimensions.

The accuracy of the results was verified by comparing with computed and measured data of a solid type resonator published by Kobayashi [13] and shown in Table I. It is shown that the

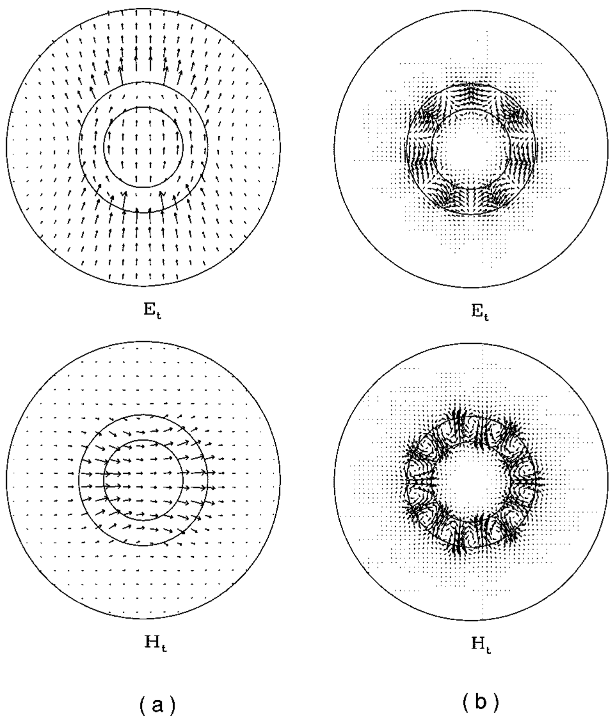

Fig. 4. Typical field distributions of the low-order mode and WGM. (a) HE_{11} mode. (b) HE_{71} mode.

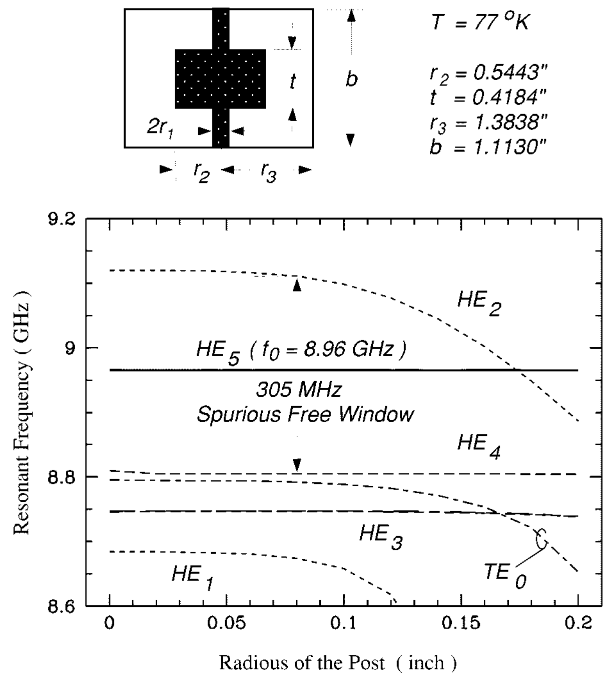

Fig. 5. Mode chart of a solid type HE_5 sapphire resonator as a function of the radius of support.

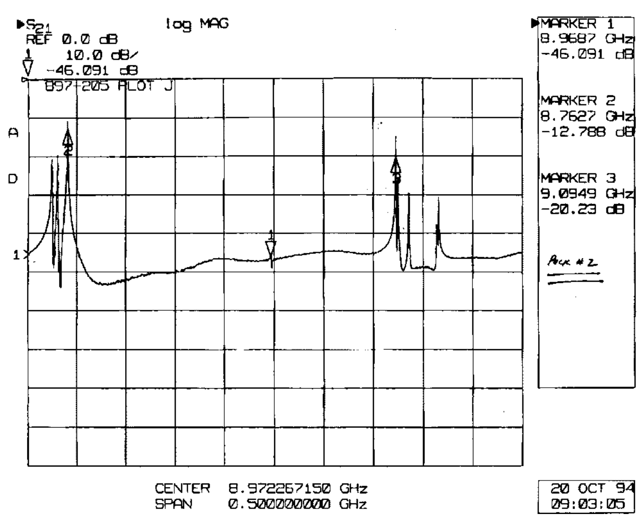

Fig. 6. Measured resonant frequency and spurious free window of the HE_5 resonator.

computed results by the present method are in excellent agreement with the numerical and experimental data, except the measured frequency of TM_{01}. This is due to the inaccuracy of the measured ϵ_z value, as explained in [13].

Fig. 4 shows the typical field distribution of the TE_{01} mode and HE_{71} mode of a sapphire resonator. It is shown that the electromagnetic field outside the sapphire resonator is relatively high for the lower order modes, As a result, the resonator's Q will degrade due to the enclosure wall loss. The electromagnetic energy in sapphire resonators operating with WGM is almost entirely confined in the dielectric region and, therefore, the Q degradation from the enclosure wall loss is minimized.

Fig. 5 shows the mode chart of an optimized solid HE_5 sapphire resonator with support as a function of the support radius. It is seen that the resonant frequencies of the HE_5 mode is nearly invariable to the change of the support radius, which implies that the resonator is highly stable. The optimized post radius is at $0.075''$, which gives 305-MHz spurious free window. The measured results of the resonant frequency and the spurious-free window of the resonator with $0.075''$ supporting post is shown in Fig. 6. Marker 1 shows the resonant frequency of the HE_5 mode, and markers 2 and 3 indicate the resonant frequencies of HE_4 and HE_2 modes, corresponding to the resonant modes in Fig. 5 at $r_1 = 0.075''$, respectively. The excellent agreement between the computed and measured results again shows the correctness of the theory and accuracy of the results.

Fig. 7 shows the typical contributions of the dielectric loss and conductive losses of a ring type WGM sapphire resonator operating at HE_5, HE_7, and HE_{11} modes as a function of temperature from 50 to 100K. The resonant frequencies of the WGM modes are 8.1, 9.6, and 13.0 GHz, respectively [12]. The unloaded Q's of the HE_7 and HE_{11} modes are mostly determined by the dielectric loss of the resonator, while the conductive loss is dominant for HE_5 mode. The computed unloaded Q's are compared with the measured results by Flory [12]. The unloaded Q's of the HE_{11} mode are close to that by the experiment. However, the measured Q's of the HE_7 mode are too low, which is probably due to the strong influence of some extrinsic loss factors [12], such as poor contact of the enclosure.

The dependence of the unloaded Q of the sapphire resonator on the size of the enclosure (r_3, b) to the size of sapphire (r_2, b_2) is presented in Fig. 8. The dielectric losses of the resonator is nearly independent on the size of the enclosure. When the

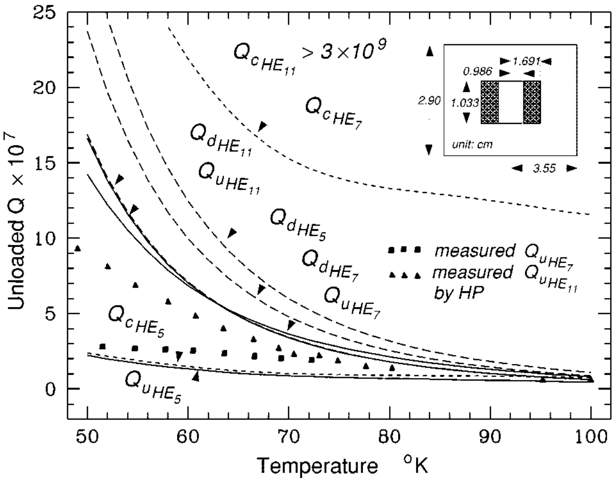

Fig. 7. Contributions of the dielectric and conductor unloaded Q of a sapphire resonator as a function of temperature.

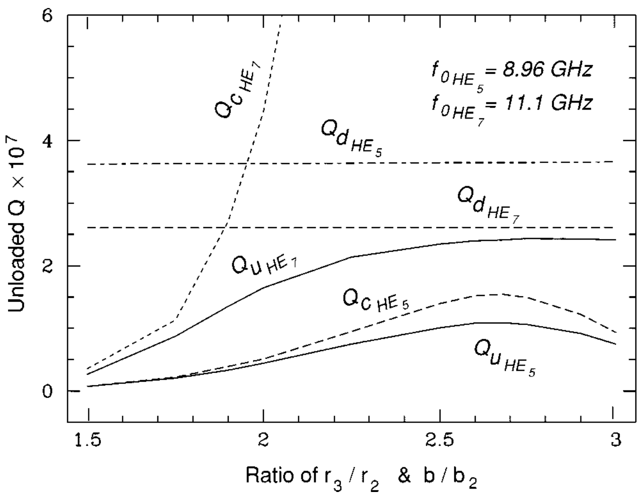

Fig. 8. Effect of the enclosure size on the unloaded Q of a sapphire resonator at 77K.

size of the enclosure is small, the conductive losses are dominant for both HE_5 and HE_7 modes. As the size of the enclosure increases, the metallic loss of the HE_7 mode decreases rapidly, and the dielectric loss is the main factor that determines the unloaded Q of the HE_7 mode. The unloaded Q of the HE_5 mode is always strongly affected by the conductive losses of the resonator. The conductive losses of the HE_5 approaches minimum value at certain size of cavity because of the field strength at the enclosure and surface area of the cavity.

Fig. 9(a) presents the computed frequency sensitivity $\Delta f/\Delta b$ of a solid-type sapphire resonator versus the height of the enclosure of both low- and high-order modes. The computed results by conventional method of computing the resonant frequencies (f_1, f_2) at different enclosure height (b_1, b_2) are also shown in the figure. It is seen that the computed results of the low-order modes by the two methods are in good agreement, which verify the correctness of the results by perturbation theory. When the order of the mode gets higher, the frequency sensitivity of the mode becomes smaller. The

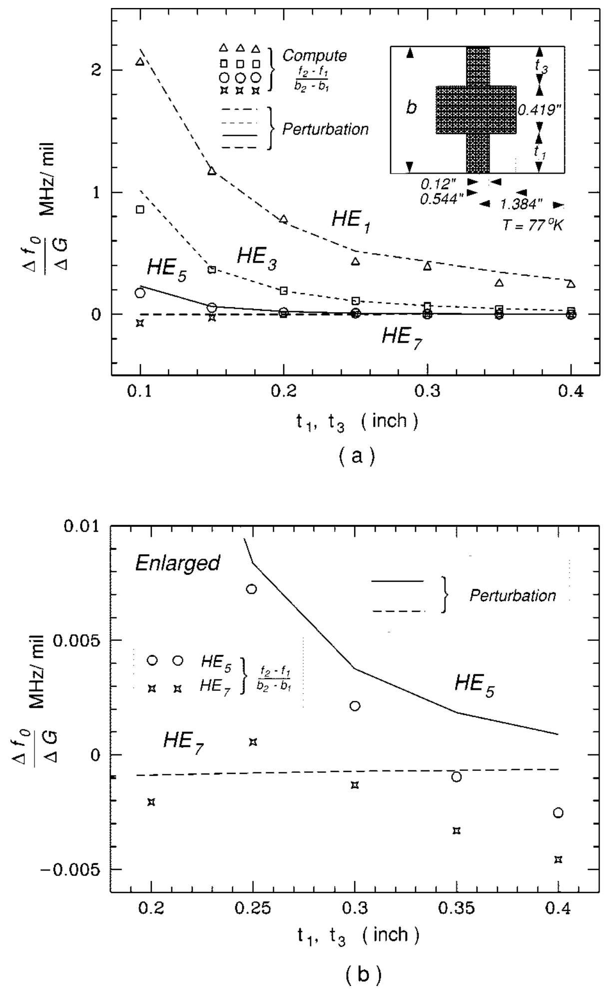

Fig. 9. Perturbation results of a sapphire resonator by changing the height of the enclosure. (a) Both low - and high-order modes. (b) Enlarged curve of the high-order modes.

enlarged figure [see Fig. 9(b)] shows that the conventional method is incapable of computing the frequency sensitivity of the higher order modes, and the perturbation method gives the correct and reliable results of both low- and high-order modes.

IV. Conclusions

A generalized multilayer cylindrical anisotropic dielectric loaded resonator is modeled by a rigorous mode-matching method. Resonant frequency, field distribution, and unloaded Q of the resonant mode are obtained. The frequency sensitivity of the higher order mode is accurately computed by incorporating the perturbation theory. The correctness of the theory and accuracy of the results are verified by comparison with other computed and measured results.

References

[1] S. B. Cohn, "Microwave bandpass filters containing high-Q dielectric resonators," *IEEE Trans. Microwave Theory Tech.*, vol. MTT-16, pp. 218–227, Apr. 1968.

[2] W. H. Harrison, "A miniature high-Q bandpass filter employing dielectric resonators," *IEEE Trans. Microwave Theory Tech.*, vol. MTT-16, pp. 210–218, Apr. 1968.

[3] S. J. Fiedziuszko, "Dual mode dielectric resonator loaded cavity filter," *IEEE Trans. Microwave Theory Tech.*, vol. MTT-30, pp. 1311–1316, Sept. 1982.

[4] S.-W. Chen and K. A. Zaki, "Dielectric ring resonators loaded in waveguide and on substrate," *IEEE Trans. Microwave Theory Tech.*, vol. 39, pp. 2069–2076, Dec. 1991.

[5] D. G. Blair and I. N. Evans, "High-Q microwave properties of a sapphire ring resonator," *J. Phys. D, Appl. Phys.*, vol. 15, pp. 1651–1656, 1982.

[6] V. B. Braginsky, V. S. Πchenko, and K. S. Bagdassarov, "Experimental observation of fundamental microwave absorption in high-quality dielectric crystals," *Phys. Lett.*, vol. A. 120, pp. 300–305, 1987.

[7] D. G. Blair and A. M. Sanson, "High Q tunable sapphire loaded cavity resonator for cryogenic operation," *Cryogenics*, vol. 29, pp. 1045–1049, 1989.

[8] G. J. Dick and J. Saunders, "Measurement and analysis of a microwave oscillator stabilized by a sapphire dielectric ring resonator for ultra-low noise," *IEEE Trans. Ultrason., Ferroelect., Freq. Contr.*, vol. 37, pp. 339–346, Sept. 1990.

[9] M. E. Tobar and A. G. Mann, "Resonant frequencies of higher order modes in cylindrical anisotropic dielectric resonators," *IEEE Trans. Microwave Theory Tech.*, vol. 39, pp. 2077–2082, Dec. 1991.

[10] M. M. Driscoll *et al.*, "Cooled, ultrahigh Q, sapphire dielectric resonators for low-noise microwave signal generation," *IEEE Trans. Ultrason., Ferroelect., Freq. Contr.*, vol. 39, pp. 405–411, May 1992.

[11] E. N. Ivanov, D. G. Blair, and V. I. Kalinichev, "Approximate approach to the design of shielded dielectric disk resonators with whispering-gallery modes," *IEEE Trans. Microwave Theory Tech.*, vol. 41, pp. 632–638, Apr. 1993.

[12] R. C. Taber and C. A. Flory, "Microwave oscillators incorporating cryogenic sapphire dielectric resonators," *IEEE Trans. Ultrason., Ferroelect., Freq. Contr.*, vol. 42, pp. 111–119, Jan. 1995.

[13] Y. Kobayashi and T. Senju, "Resonant modes in shielded uniaxial-anisotropic dielectric rod resonators," *IEEE Trans. Microwave Theory Tech.*, vol. 41, pp. 2198–2205, Dec. 1993.

[14] J. F. Liang, C. Wang, Q. F. Sun, and K. A. Zaki, "Supporting structure's effects on high Q dielectric resonators for oscillator applications," in *IEEE Int. Freq. Contr. Symp. Dig.*, Sept. 1994, pp. 478–491.

Chi Wang (S'95–A'97–SM'98) received the B.S. and the M.S. degrees from the Beijing Institute of Technology, Beijing, China, in 1983 and 1986, respectively, and the Ph.D. degree from the University of Maryland at College Park, in 1997, all in electrical engineering.

From 1986 to 1989, he was an Electrical Engineer at North China Vehicle Research Institute, Beijing, China, where he was engaged in developing an auto test system. From 1990 to 1992, he was with Beijing XYE Electronics Inc., Beijing, China, where he was involved with RF circuit and system design. He spent one year as a Research Associate at the Beijing Institute of Technology , where he was involved with modeling of antennas and resonators using the finite-difference time-domain method. From 1994 to 1997, he held a Graduate Research Assistantship with the Microwave Research Group, University of Maryland at College Park, where he was involved with the analysis, modeling, and design of microwave circuits and devices. From 1994 to 1995, he was also a Graduate Teaching Assistant. Since November 1997, he has been with Celwave (a division of Radio Frequency Systems Inc.), Marlboro, NJ, where he is involved with RF/microwave devices and systems.

Kawthar A. Zaki (SM'85–F'91) received the B.S. degree with honors from Ain Shams University, Cairo, Egypt, in 1962, and the M.S. and the Ph.D. degrees from the University of California at Berkeley, in 1966 and 1969, respectively, all in electrical engineering.

From 1962 to 1964, she was a Lecturer in the Department of Electrical Engineering, Ain Shams University. From 1965 to 1969, she was a Research Assistant in the Electronics Research Laboratory, University of California at Berkeley. In 1970, she joined the Electrical Engineering Department, University of Maryland at College Park, where she is currently a Professor of electrical engineering. Her research interests are in the areas of electromagnetics, microwave circuits, simulation, optimization, and computer-aided design of advanced microwave and millimeter-wave systems and devices. She has authored or co–authored over 200 publications in her areas of research interest, and holds five patents on filters and dielectric resonators.

Dr. Zaki has been the recipient of several academic honors and awards for teaching, research, and inventions.